Physica D 340 (2017) 1–13

Contents lists available at ScienceDirect

Physica D

journal homepage: www.elsevier.com/locate/physd

Windows of opportunity for synchronization in stochastically coupled maps

Olga Golovneva [a], Russell Jeter [b], Igor Belykh [b,*], Maurizio Porfiri [a,*]

[a] Department of Mechanical and Aerospace Engineering, New York University Tandon School of Engineering, Brooklyn, NY 11201, USA
[b] Department of Mathematics and Statistics and Neuroscience Institute, Georgia State University, Atlanta, GA 30303, USA

HIGHLIGHTS

- We study synchronization of stochastically coupled one-dimensional maps.
- Non-fast switching conditions are analytically and numerically investigated.
- We prove the existence of windows of opportunity for the switching period.
- We formulate mathematically-tractable necessary conditions for synchronization.
- For tent maps, a closed-form expression for the Lyapunov exponent is derived.

GRAPHICAL ABSTRACT

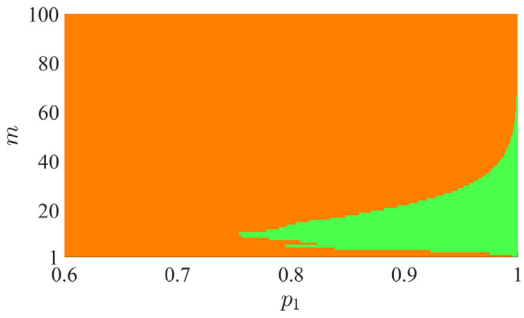

Demonstration of emergence of windows of opportunity in a pair of stochastically coupled tent maps. The "Pinocchio nose" shows pairs of switching periods (m) and probabilities (p_1) where synchronization is attained.

ARTICLE INFO

Article history:
Received 24 March 2016
Received in revised form
24 June 2016
Accepted 18 August 2016
Available online 1 September 2016
Communicated by K. Josic

Keywords:
Networks
Stochastic stability
Switching
Synchronization
Windows of opportunity

ABSTRACT

Several complex systems across science and engineering display on–off intermittent coupling among their units. Most of the current understanding of synchronization in switching networks relies on the fast switching hypothesis, where the network dynamics evolves at a much faster time scale than the individual units. Recent numerical evidence has demonstrated the existence of windows of opportunity, where synchronization may be induced through non-fast switching. Here, we study synchronization of coupled maps whose coupling gains stochastically switch with an arbitrary switching period. We determine the role of the switching period on synchronization through a detailed analytical treatment of the Lyapunov exponent of the stochastic dynamics. Through closed-form expressions and numerical findings, we demonstrate the emergence of windows of opportunity and elucidate their nontrivial relationship with the stability of synchronization under static coupling. Our results are expected to provide a rigorous basis for understanding the dynamic mechanisms underlying the emergence of windows of opportunity and leverage non-fast switching in the design of evolving networks.

1. Introduction

Dynamical systems with a network structure arise naturally as models in many fields, including physics, biology, engineering, and social sciences [1–5]. Significant attention has been devoted to un-

* Corresponding authors.
E-mail addresses: ibelykh@gsu.edu (I. Belykh), mporfiri@nyu.edu (M. Porfiri).

http://dx.doi.org/10.1016/j.physd.2016.08.005
0167-2789/

derstand the role of and interplay between node dynamics and network structure, specifically in regard to network synchronization, see, for example, [6–13].

While most of the literature has focused on static networks, many examples of technological and natural networks are more accurately described through dynamic networks, where individual nodes interact through time-varying coupling [10,14–32]. Of particular interest are "blinking" networks [33–37], in which connections switch on and off randomly, modulating the collective dynamics of the interacting nodes. Examples of stochastically switching networks include packet-switched networks (the Internet) [38], switching power converters [39], ecological networks with sporadic dispersal [40], epidemiological networks [41], and animal grouping [42].

For example, synchronization of computer clocks over the Internet is achieved via sporadic on–off signals whose switching frequency is governed by a trade-off between the precision of synchronization and the traffic load on the network [38]. Stochastic switching in power converters helps distribute the power of the parasitic frequency components over a wider frequency range [39]. In many ecological networks, the coupling among the patches is sporadic/stochastic, due to rare and short-term meteorological conditions. However, spatial synchrony, increasing the danger of extinction, can robustly appear, even though the patches are disconnected most of the time [40]. The structure of epidemiological networks of moving individuals is essentially time-varying and stochastic, and the propagation of a disease depends on proximity among infected and susceptible moving agents [41]. In animal grouping, schools of fish are a representative example of a stochastic time-varying network, where each fish has access only to its neighbors which randomly change in time during schooling [42]. All of these networks belong to a wide class of *evolving dynamical networks* whose study and control have yet to be fully elucidated, see the recent review paper [7] and references therein.

"Blinking" networks were originally introduced for *continuous-time* oscillators in the context of network synchronization in [33]. Over the years, we have investigated various aspects of synchronization in blinking networks of continuous-time [33,34,36,37,43–47] and discrete-time [48–57] oscillators. In particular, it was rigorously proven in both continuous and discrete-time cases that if the switching frequency is sufficiently high, with respect to the characteristic time of the individual oscillators ("fast switching limit"), the stochastically blinking network can synchronize even if the network is disconnected at every instant of time.

Beyond synchronization, a rigorous theory for the behavior of stochastic switching networks of continuous-time oscillators in the fast switching limit was developed in [58–60]. These studies have helped in clarifying a number of counterintuitive findings on the relationship between the stochastic network and its time-averaged counterpart, where the dynamical law is given by the expectation of the stochastic variables. While our intuition suggests that the switching network should follow the averaged system in the fast switching limit, this is not always the case, especially when the averaged system is multistable and its attractors are not invariant under the switching system. These attractors act as ghost attractors for the switching system, whereby the trajectory of the switching system can only reach a neighborhood of the ghost attractor, and remains close most of the time with high probability when switching is fast. In a multistable system, the trajectory may escape to another ghost attractor with low probability [58]. This theory uses the Lyapunov function method along with large deviation bounds to derive explicit conditions that connect the probability of converging toward an attractor of a multistable blinking network, the fast switching frequency, and the initial conditions [58]. As the switching frequency decreases, it was shown that there is a range of "resonant" frequencies where the trajectory of a multistable switching oscillator receives enough kicks in the wrong direction to escape from the ghost attractor against all odds [58].

In the context of continuous-time blinking networks, similar unexpected windows of non-fast switching frequencies were found in Rössler and Duffing oscillators [61] and tritrophic Rosenzweig–MacArthur food-chain models [40]. These regions, called "windows of opportunity" [40,61], correspond to the emergence of stable synchronization in the switching network over bounded intervals of the switching frequency, which may not include the fast switching limit. As a result, networks that do not synchronize in the fast switching limit may synchronize for non-fast switching, and then lose synchronization as the frequency is further reduced. Observed numerically, this phenomenon calls for a more rigorous study to isolate the principal mechanisms underpinning unexpected synchronization from non-fast switching. This paper aims at establishing such an analytical insight.

We focus on a *discrete-time* setting, where the coupling between the maps is held fixed for a finite number of time steps (switching period) and then it stochastically switches, independent of the time history. In this case, non-fast switching can be tackled by re-scaling the time variable and consequently modifying the individual dynamics of the coupled maps. This enables the formulation of a rigorous mathematical framework for the analysis of the stochastic stability of synchronization as a function of the switching period. We restrict our analysis to two one-dimensional (1D) coupled maps with the two-fold aim of: (i) providing a clear demonstration for the origin of this phenomenon, which may be hidden by topological factors in large networks, and (ii) establishing a toolbox of closed-form results for the emergence of windows of opportunity.

We study the stability of synchronization by analyzing the linear stability of an augmented system, associated with the linear mean square transverse dynamics. We perform a detailed analysis of the Lyapunov exponent of the transverse dynamics, based on the knowledge of the probability density function for the synchronized trajectory. We establish a necessary condition for stochastic synchronization in terms of the synchronizability of the coupled maps with a static coupling. The necessary condition can be used to demonstrate that switching between configurations which do not individually support synchronization will not stabilize stochastic synchronization for any switching frequencies. This is in contrast with networks of continuous-time oscillators where windows of opportunity for stable synchronization may appear as a result of switching between *unstable states* [40,61,62].

To illustrate our approach, we use the paradigm of two linearly coupled "sigmoid" maps, which encompasses the traditional logistic and tent maps. Statically coupled tent maps are known to have two symmetric ranges of positive and negative coupling for which synchronization is locally stable [63], and a similar behavior is observed for their smooth versions in the form of sigmoid maps. In our setting, we let the coupling stochastically switch between values within and outside these stability regions to explore the emergence of windows of opportunity. We demonstrate that while fast switching, occurring at each time step, may not synchronize the maps, there can be a range of lower frequencies that yields stable synchronization. We argue that this is possible for coupled maps where the probability of switching between stable and unstable configurations is uneven, inducing a non-trivial balance between the dynamics of the coupled maps and the switching periods.

The layout of this paper is as follows. First, in Section 2, we present the stochastic model of coupled maps and introduce the mean square stability of the transverse dynamics. In Section 3, we establish a mathematically-tractable form for the Lyapunov

exponent of the stochastic dynamics, which unveils its relationship with the stability of synchronization when the maps are statically coupled. We discuss the case when the individual map has a fixed point and then turn to periodic and chaotic dynamics. We derive a necessary condition for stochastic synchronization, implicitly involving the switching period required for stable synchronization. In Section 4, we study in detail the case of coupled sigmoid maps through both analysis and numerics. In Section 5, a brief discussion of the obtained results is given. Appendix A contains the description of the sigmoid map along with its probability density function. Finally, Appendix B presents the derivation of the closed-form expression of the Lyapunov exponent of stochastically coupled tent maps used to reveal windows of opportunity.

2. Linear stability of synchronization under stochastic switching

2.1. Problem statement

We study the stochastic synchronization of two 1D maps characterized by the state variables $x_i \in \mathbb{R}$, $i \in \{1, 2\}$. We assume that the individual dynamics of each node evolves according to $x_i(k+1) = F(x_i(k))$, where $k \in \mathbb{Z}^+$ is the time step and $F : \mathbb{R} \to \mathbb{R}$ is a smooth nonlinear scalar function. The maps are linearly coupled through the stochastic gains $\varepsilon_1(k), \varepsilon_2(k) \in \mathbb{R}$, such that

$$\begin{bmatrix} x_1(k+1) \\ x_2(k+1) \end{bmatrix} = \begin{bmatrix} F(x_1(k)) + \varepsilon_1(k)(x_2(k) - x_1(k)) \\ F(x_2(k)) + \varepsilon_2(k)(x_1(k) - x_2(k)) \end{bmatrix}. \tag{1}$$

Each of the sequences of coupling gains, $\varepsilon_1(0), \varepsilon_1(1), \varepsilon_1(2), \ldots$ and $\varepsilon_2(0), \varepsilon_2(1), \varepsilon_2(2), \ldots$, is assumed to be switching stochastically at the same period $m \in \mathbb{Z}^+ \setminus \{0\}$. Every m time steps, the coupling gains simultaneously switch, such that $\varepsilon_1(mk) = \varepsilon_1(mk+1) = \cdots = \varepsilon_1(mk+m-1) = \tilde{\varepsilon}_1(k)$ and $\varepsilon_2(mk) = \varepsilon_2(mk+1) = \cdots = \varepsilon_2(mk+m-1) = \tilde{\varepsilon}_2(k)$ for every time step k, where $\tilde{\varepsilon}_1(0), \tilde{\varepsilon}_1(1), \ldots$ and $\tilde{\varepsilon}_2(0), \tilde{\varepsilon}_2(1), \ldots$ are two sequences of independent identically distributed random variables.

The evolution of the coupled maps in Eq. (1) is determined by the random variables $\tilde{\varepsilon}_1$ and $\tilde{\varepsilon}_2$, from which the coupling gains are drawn. In general, these random variables may be related to each other and may not share the same distribution. For example, in the case of one-directional stochastic coupling, one of the random variables is zero; on the other hand, for bi-directional interactions, the two random variables coincide.

The current state of knowledge on stochastic synchronization of coupled discrete maps is largely limited to the case $m = 1$, for which the coupling gains switch at every time step [7]. In this case, the random variables $\varepsilon_i(0), \varepsilon_i(1), \varepsilon_i(2), \ldots$, for $i \in \{1, 2\}$, are mutually independent. For each value of k, $x_1(k+1)$ and $x_2(k+1)$ are functions only of the previous values $x_1(k)$ and $x_2(k)$, and Eq. (1) reduces to a first order Markov chain with explicit dependence on time through the individual dynamics. In the case of $m > 1$, the random variables $\varepsilon_i(0), \varepsilon_i(1), \varepsilon_i(2), \ldots$, for $i \in \{1, 2\}$, are no longer independent, which poses further technical challenges for the analysis of the system, while opening the door for rich behavior to emerge from the stochastically driven coupling.

The oscillators synchronize at time step k if their states are identical, that is, $x_1(k) = x_2(k)$. From Eq. (1), once the oscillators are synchronized at some time step, they will stay synchronized for each subsequent time step. The common synchronized trajectory $s(k)$ is a solution of the individual dynamics, whereby $s(k+1) = F(s(k))$. The linear stability of synchronization can be studied through the following variational equation, obtained by linearizing Eq. (1) in the neighborhood of the synchronization manifold:

$$\xi(k+1) = \left[F'(s(k)) - d(k)\right]\xi(k), \tag{2}$$

where prime indicates differentiation, $d(k) = \varepsilon_1(k) + \varepsilon_2(k)$ is the net coupling, and $\xi(k) = x_1(k) - x_2(k)$ is the synchronization error at time step k. Eq. (2) defines the linear transverse dynamics of the coupled oscillators, measured with respect to the difference between their states $\xi(k)$. This quantity is zero when the two oscillators are synchronized. Eq. (2) rests on the assumption that the mapping governing the individual dynamics, F, is differentiable everywhere. This assumption can be relaxed, however, to functions that are differentiable almost everywhere [64].

Only the sum of the two coupling gains $\varepsilon_1(k)$ and $\varepsilon_2(k)$ affects the transverse dynamics, thereby only the statistics of the random variable $d(k)$ modulate the linear stability of the synchronization manifold. To simplify the treatment of the variational problem in Eq. (2), we can re-scale the time variable with respect to the switching period as follows:

$$\tilde{\xi}(k+1) = \prod_{i=0}^{m-1} (F'(s(mk+i)) - \tilde{d}(k))\tilde{\xi}(k), \tag{3}$$

where $\tilde{\xi}(k) = \xi(mk)$ and $\tilde{d}(k) = \tilde{\varepsilon}_1(k) + \tilde{\varepsilon}_2(k)$. Eq. (3) casts the variational dynamics in the form of a first order time-dependent Markov chain, generated by a linear time-varying stochastic finite difference equation [65,66].

It is important to emphasize that the synchronization manifold $x_1(k) = x_2(k)$ is an invariant set of the stochastic equation (1). Therefore, the dynamics on the synchronization manifold is governed by an attractor which is also invariant under the flow of the stochastic system, such that its existence is defined via the individual deterministic map. Therefore, we can assume the existence of the synchronous solution $s(k)$ without any additional proof. In this context, system (3) with stochastically switching coupling gains differs from a general random dynamical system where the definition of an attractor is not straightforward and requires the notion of invariant measure and space averages. While the synchronous dynamics in the stochastic Eq. (1) is deterministic, the convergence to the synchronization manifold is governed by the stochastic switching process. In the following, we analyze this stochastic convergence to ascertain stable stochastic synchronization.

2.2. Mean square stability of synchronization

In determining the stability of the synchronous state, various criteria can be considered, such as almost sure, in probability, and mean square [65,66]. The concept of mean square stability is particularly attractive, due to its practicality of implementation and its inclusiveness with respect to other criteria. Mean square stability of the synchronous state is ascertained through the analysis of the temporal evolution of the second moment of the error $\mathrm{E}[\tilde{\xi}^2]$, where $\mathrm{E}[\cdot]$ indicates expectation with respect to the σ-algebra generated by the switching. By taking the square of each side of Eq. (3) and computing the expectation, we obtain

$$\mathrm{E}\left[\tilde{\xi}^2(k+1)\right] = \mathrm{E}\left[\prod_{i=0}^{m-1} (F'(s(mk+i)) - \tilde{d}(k))^2\right] \mathrm{E}\left[\tilde{\xi}^2(k)\right]. \tag{4}$$

The above recursion is a linear, time-varying, deterministic finite difference equation whose initial condition is $\tilde{\xi}^2(0)$, which is treated as a given value and not as a random variable. We say that Eq. (3) is mean square asymptotically stable if Eq. (4) is asymptotically stable, that is, if the Lyapunov exponent λ of Eq. (4) is negative. This implies that any small difference between the states of the oscillators will converge to zero in the mean square sense as time increases.

Eq. (4) is based on the assumption that switching is memoryless, such that the first expectation on the right hand side is not

conditioned with respect to the previous time step. Extending the analysis to switching with memory could be addressed by augmenting the error dynamics with the net coupling gain. This effort will be the object of future studies.

The Lyapunov exponent is a function of the switching period m and can be computed from Eq. (4) as follows [64]:

$$\lambda(m) = \lim_{k\to\infty} \frac{1}{k} \ln \prod_{j=0}^{k-1} \mathrm{E}\left[\prod_{i=0}^{m-1} (F'(s(mj+i)) - \tilde{d}(j))^2\right]. \tag{5}$$

In general, the stability of the synchronization manifold depends on the underlying synchronous solution, whereby $\lambda(m)$ in Eq. (5) explicitly depends on $s(k)$. In what follows, we focus on the case where $s(k)$ is a fixed point of the individual map, a periodic trajectory, or a chaotic trajectory. We comment that our approach is based on the linearized dynamics in Eq. (2), which requires small perturbations near the synchronous state. Thus, our analysis is only applicable to the study of local stability of the synchronization manifold, and initial conditions cannot be arbitrarily selected in the basin of attraction.

3. Main results

We assume that $\tilde{d}(k)$ takes values on a finite sample space $D = \{d_1, d_2, \ldots, d_n\}$ of cardinality n. For $l = 1, \ldots, n$, the probability that the net coupling is equal to d_l is chosen to be equal to p_l. For example, in the case of simple on–off connections, the individual coupling gains take values 0 and ε with corresponding probabilities p and $1-p$. Therefore, the net coupling gain $\tilde{d}(k)$ takes values $d_1 = 0$, $d_2 = \varepsilon$, and $d_3 = 2\varepsilon$ with corresponding probabilities $p_1 = p^2$, $p_2 = 2p(1-p)$ and $p_3 = (1-p)^2$.

From the individual values of the net coupling and their probabilities, we can evaluate the Lyapunov exponent in Eq. (5) as

$$\lambda(m) = \lim_{k\to\infty} \frac{1}{k} \sum_{j=0}^{k-1} \ln\left[\sum_{l=1}^{n} p_l \prod_{i=0}^{m-1} (F'(s(mj+i)) - d_l)^2\right]. \tag{6}$$

One of the central objectives of this study is to understand the relationship between the synchronizability of the coupled maps when statically coupled through the net coupling gains in D and their stochastic synchronizability when the net coupling randomly switches at a period m. To this end, we adjust Eq. (6) to the case of statically coupled maps with a net coupling $d^\star$

$$\lambda^{\mathrm{st}}(d^\star) = \lim_{k\to\infty} \frac{1}{k} \sum_{j=0}^{k-1} \ln\left[(F'(s(j)) - d^\star)^2\right]. \tag{7}$$

For convenience, we write $\lambda_l^{\mathrm{st}} = \lambda^{\mathrm{st}}(d_l)$ for $l = 1, \ldots, n$. Depending on the value of d_l, the statically coupled systems may synchronize or not, that is, the corresponding error dynamics may be asymptotically stable or unstable.

In what follows, we first establish a relationship between the Lyapunov exponents associated with the statically coupled maps and the Lyapunov exponent of the stochastic dynamics. We leverage this relationship to formulate a necessary condition for stochastic synchronization, which only requires knowledge of the statically coupled maps. Next, we explore the connection between the averaged system, which is at the core of the fast switching literature, and stochastic synchronization. Finally, we demonstrate the approach to the study of synchronization about fixed points and periodic or chaotic dynamics. For fixed points, we show the feasibility of a single window of opportunity in relation to the stability properties of each coupling configuration. For periodic or chaotic dynamics, a similar, general treatment is problematic. Thus, we propose an analytical approach for maps with known probability density function, on which we base the closed-form computation of stochastic Lyapunov exponents for coupled tent maps, detailed in Appendix B.

3.1. Relating Lyapunov exponents of statically and stochastically coupled maps

If all of the Lyapunov exponents of the statically coupled systems are finite, then we can establish the following relationship between the Lyapunov exponent of the stochastic error dynamics (6) and $\{\lambda_r^{\mathrm{st}}\}_{r=1}^n$:

$$\lambda(m) = m\lambda_r^{\mathrm{st}} + \lim_{k\to\infty} \frac{1}{k} \sum_{j=0}^{k-1} \ln\left[\frac{\sum_{l=1}^{n} p_l \prod_{i=0}^{m-1} (F'(s(mj+i)) - d_l)^2}{\prod_{i=0}^{m-1} (F'(s(mj+i)) - d_r)^2}\right], \tag{8}$$

for $r = 1, \ldots, n$. Eq. (8) is derived from Eq. (6) by: (i) dividing and multiplying the argument of the logarithm by $\prod_{i=0}^{m-1}(F'(s(mj+i)) - d_r)^2$; (ii) using the product rule of logarithms; and (iii) applying Eq. (7) upon re-scaling the time variable by the period m. We note that if $p_r = 1$, such that the coupling does not switch, $\lambda(m) = m\lambda_r^{\mathrm{st}}$; the dependence on m is due to the time re-scaling in Eq. (3).

By multiplying both sides of Eq. (8) by p_r and summing over r, we obtain the following compact relationship between the Lyapunov exponent of the stochastic dynamics and the individual Lyapunov exponents for statically coupled maps:

$$\lambda(m) = m \sum_{l=1}^{n} p_l \lambda_l^{\mathrm{st}} + \lim_{k\to\infty} \frac{1}{k} \sum_{j=0}^{k-1} \ln \frac{\sum_{l=1}^{n} p_l \zeta_l(j)}{\prod_{l=1}^{n} \zeta_l^{p_l}(j)}. \tag{9}$$

Here, we have introduced:

$$\zeta_l(j) = \prod_{i=0}^{m-1} (F'(s(mj+i)) - d_l)^2, \tag{10}$$

which we assume to be different than zero to ensure that the Lyapunov exponent stays finite.

The first summand on the right-hand side of Eq. (9) is linearly proportional to the switching period m and the "effective" Lyapunov exponent $\bar{\lambda} = \sum_{l=1}^{n} p_l \lambda_l^{\mathrm{st}}$, which corresponds to the average of the Lyapunov exponents associated with the statically coupled maps, weighted by the probability of the corresponding switching. The second summand on the right-hand side of Eq. (9) is a residual quantity, which encapsulates the complex dependence of the transverse dynamics on the switching period beyond the linear dependence associated with the first summand.

A lower bound for the Lyapunov exponent $\lambda(m)$ can be obtained by applying the weighted arithmetic–geometric mean inequality [67]

$$\prod_{l=1}^{n} \zeta_l^{p_l} \leqslant \sum_{l=1}^{n} p_l \zeta_l. \tag{11}$$

From inequality (11), it follows that the argument of the logarithm in Eq. (9) is larger than or equal to 1, such that the second summand therein is always nonnegative. As a result, we obtain

$$\lambda(m) \geqslant m\bar{\lambda}. \tag{12}$$

This inequality[1] establishes that for $\lambda(m)$ to be negative, $\bar{\lambda}$ must also be negative. Thus, we are ready to state the following necessary condition for stochastic synchronization.

[1] For chaotic dynamics, the inequality is always strict, whereby the weighted arithmetic and geometric mean, introduced in (11), are equal if and only if $\zeta_1 =$

Proposition 1. *The synchronization of the stochastic system (1) is mean square stable only if the effective Lyapunov exponent $\bar{\lambda}$ is negative.*

This proposition implies that if none of the Lyapunov exponents $\{\lambda_r^{\rm st}\}_{r=1}^n$ is negative, synchronization is not feasible for any selection of m and $\{p_r\}_{r=1}^n$. Thus, stochastic synchronization cannot be achieved without at least one coupling configuration that supports synchronization. This is in contrast with observations on continuous-time systems which indicate the possibility of stable synchronization even if none of the coupling configurations support synchronization [40,61].

3.2. Can we infer stochastic synchronization from the averaged system?

For continuous-time systems, in our previous work [33,34,36,37,43–47] we have shown that under fast switching conditions the synchronizability of the stochastically switching system can be assessed from the synchronizability of the averaged system, where the stochastic coupling is replaced by its time-average. Here, we re-examine this limit in the case of coupled maps, whereby the averaged system is obtained by replacing the switching gain by its expected values. The synchronizability of the averaged system is ascertained by studying the Lyapunov exponent obtained by replacing $d^\star$ with $\mathrm{E}[d]$ in Eq. (7), that is,

$$\lambda^{\rm aver} = \lim_{k\to\infty} \frac{1}{k} \sum_{j=0}^{k-1} \ln\left[(F'(s(j)) - \mathrm{E}[d])^2\right]. \tag{13}$$

3.2.1. Not in general

Here, we demonstrate through examples that the weighted average Lyapunov exponent $\bar{\lambda}$ can be positive or negative, *independent* of the value of $\lambda^{\rm aver}$. Therefore, the averaged system does not offer valuable insight on the stability of the synchronization manifold of the stochastically coupled maps. For the sake of illustration, we consider the case in which the individual dynamics corresponds to the identity, such that

$$\begin{bmatrix} x_1(k+1) \\ x_2(k+1) \end{bmatrix} = \begin{bmatrix} x_1(k) + \varepsilon_1(k)(x_2(k) - x_1(k)) \\ x_2(k) + \varepsilon_2(k)(x_1(k) - x_2(k)) \end{bmatrix}. \tag{14}$$

In this case, the transverse dynamics in (2) takes the simple form

$$\xi(k+1) = [1 - d(k)]\,\xi(k). \tag{15}$$

Statically coupled identity maps should have a Lyapunov exponent given by (7) with $F'(s(j)) = 1$, that is,

$$\lambda^{\rm st}(d^\star) = \ln\left[(1-d^\star)^2\right]. \tag{16}$$

Suppose that the net switching gain is a random variable that takes values $d_1 = 1$ and $d_2 = -1$ with equal probabilities 0.5. Then, using Eq. (16) we compute

$$\bar{\lambda} = \frac{1}{2}\left(\lambda^{\rm st}(1) + \lambda^{\rm st}(-1)\right) = -\infty, \tag{17a}$$

$$\lambda^{\rm aver} = \lambda^{\rm st}(0) = 0 > \bar{\lambda}. \tag{17b}$$

Thus, the average coupling does not support synchronization, even though the effective Lyapunov exponent is negative.

Now, we assume $d_1 = 0$ and $d_2 = 2$ with the same probability 0.5, which yields

$$\bar{\lambda} = \frac{1}{2}\left(\lambda^{\rm st}(0) + \lambda^{\rm st}(2)\right) = 0, \tag{18a}$$

$$\lambda^{\rm aver} = \lambda^{\rm st}(1) = -\infty < \bar{\lambda}. \tag{18b}$$

This posits that the stochastically coupled maps cannot synchronize for any selection of the period m, even though the average coupling affords synchronization in a single time step.

3.2.2. Yes, for coupling gains which are close to each other

If the difference between the possible values of the net coupling gain in D is sufficiently small, the stability of the stochastic system can be related to the stability of the error dynamics of the averaged system. In this case, if for all $l = 1, \ldots, n$, we can write $F'(x) - d_l$ as $F'(x) - \mathrm{E}[d] + \Delta d_l$, where $|\Delta d_l| \ll |F'(x) - \mathrm{E}[d]|$ is the deviation of the stochastic switching with respect to their expected value. Thus, we obtain

$$\begin{aligned}\bar{\lambda} &= \sum_{l=1}^n p_l \lim_{k\to\infty} \frac{1}{k} \sum_{j=0}^{k-1} \ln\left[(F'(s(j)) - \mathrm{E}[d] + \Delta d_l)^2\right] \\ &\approx \lim_{k\to\infty} \frac{1}{k} \sum_{j=0}^{k-1} \left(\ln\left[(F'(s(j)) - \mathrm{E}[d])^2\right]\right) \\ &\quad + \sum_{l=1}^n \lim_{k\to\infty} \sum_{j=0}^{k-1} \frac{2p_l \Delta d_l}{F'(s(j)) - E[d]} = \lambda^{\rm aver},\end{aligned} \tag{19}$$

where we have expanded the logarithm in series in the neighborhood of $F'(s(j)) - \mathrm{E}[d]$ and we have used the fact that $\sum_{l=1}^n p_l \Delta d_l = 0$ by construction.

3.3. Stochastic synchronization at fixed points

We start the analysis by considering synchronization at a fixed point s_0, that is, $s_0 = F(s_0)$. In this case, the computation of the Lyapunov exponent for the stochastically coupled system in Eq. (6) can be simplified as

$$\lambda(m) = \ln\left[\sum_{l=1}^n p_l e^{m\lambda_l^{\rm st}}\right], \tag{20}$$

where the Lyapunov exponents of the statically coupled maps are given by Eq. (7), which takes the following form:

$$\lambda_l^{\rm st} = \ln\left[(F'(s_0) - d_l)^2\right]. \tag{21}$$

Depending on the value of the Lyapunov exponents of the statically coupled maps (21) and the probabilities of occurrence of the corresponding gains, we classify three distinct behaviors of the function $e^{\lambda(m)} = \sum_{l=1}^n p_l e^{m\lambda_l^{\rm st}}$, given by the argument of the logarithm in (20), as shown in Fig. 1. The existence of these three behaviors can be demonstrated by considering m as a real variable. First, we note that $e^{\lambda(m)}$ is a convex function in m, since its second derivative with respect to m is nonnegative. As m goes to 0, $e^{\lambda(m)}$ tends to 1 and its slope approaches $\bar{\lambda}$. As m goes to infinity $e^{\lambda(m)}$ will grow unbounded if there is a net coupling gain with nonzero probability that would not support synchronization.

Thus, if the coupling switches between states such that $\lambda_l^{\rm st} < 0$ for all $l = 1, 2, \ldots, n$, $\lambda(m)$ will decrease with m and will always be negative (Fig. 1(a)). This corresponds to a system that stochastically switches between coupling gains which would individually lead to synchronization for statically coupled maps. In the case of maps of a higher dimension, a similar finding should

---

$\zeta_2 = \cdots = \zeta_n$. Thus, inequality (12) reduces to an equality if and only if

$$\begin{aligned}\prod_{i=0}^{m-1} (F'(s(mj+i)) - d_1)^2 &= \prod_{i=0}^{m-1} (F'(s(mj+i)) - d_2)^2 \\ &= \cdots = \prod_{i=0}^{m-1} (F'(s(mj+i)) - d_n)^2\end{aligned}$$

holds for any $j \in \mathbb{Z}^+$, which cannot be fulfilled by aperiodic dynamics.

not be expected given the possibility of complex, non-commuting eigenstructures [68]. On the other hand, if the coupling switches between values such that $\bar{\lambda} > 0$, $\lambda(m)$ will always be positive and will increase with m (Fig. 1(b)).

Finally, if the system has at least one coupling gain corresponding to $\lambda_l^{\text{st}} > 0$, but $\bar{\lambda} < 0$, we may observe a window of opportunity. Specifically, if $e^{\lambda(1)} < 1$, the stochastically coupled maps will synchronize for $m = 1, \ldots, m^{\text{cr}}-1$, where m^{cr} is the lowest integer such that $e^{\lambda(m^{\text{cr}})} > 1$, and will not synchronize for larger switching periods (Fig. 1(c)). Notably, such a window of opportunity must encompass the fast switching limit, $m = 1$, and disconnected windows are not feasible. For chaotic dynamics, we demonstrate that both these constraints can be relaxed, with disconnected windows of opportunity extending beyond the fast switching limit.

3.4. Stochastic synchronization for periodic and chaotic dynamics

Direct computation of the Lyapunov exponent as a limit of a time series from Eq. (6) or (9) may be challenging or even not feasible; for example, if $F'(x)$ is undefined on a finite set of points x. Following the approach of [63], we replace the summation with integration using Birkhoff's ergodic theorem [69].

Toward this aim, we introduce $\rho(x)$ as the probability density function of the map $F(x)$, defined on a set B and continuously differentiable on B except for a finite number of points. We use such a density as a proxy for the long-run behavior of the stochastic system when applying Birkhoff's theorem. The probability density function of a generic map can be found analytically or numerically [70,71]. Thus, Eqs. (6), (7), and (9) can be written as

$$\lambda_l^{\text{st}} = \int_B \ln\left[(F'(t) - d_l)^2\right] \rho(t)dt, \tag{22a}$$

$$\lambda(m) = \int_B \ln\left[\sum_{l=1}^{n} p_l Y_l(t, m)\right] \rho(t)dt, \tag{22b}$$

$$\lambda(m) = m\sum_{l=1}^{n} p_l \lambda_l^{\text{st}} + \int_B \ln\left[\frac{\sum_{l=1}^{n} p_l Y_l(t, m)}{\prod_{l=1}^{n} Y_l^{p_l}(t, m)}\right] \rho(t)dt. \tag{22c}$$

Here, we have introduced the function of time and switching period

$$Y_l(t, m) = \prod_{i=0}^{m-1} (F'(F^i(t)) - d_l)^2, \tag{23}$$

where $F^i(t) = [F \circ F \circ \cdots \circ F](t)$ is the composite function of order i.

Equation set (22) can be used to explore the synchronizability of an N-periodic trajectory $s(Nk+i) = s_i$, where $i = 0, 1, \ldots, N-1$, $k \in \mathbb{Z}^+$, and $N \in \mathbb{Z}^+/\{0\}$, by using the appropriate probability density function [71] $\rho(s) = \frac{1}{N}\sum_{i=0}^{N-1} \delta(s - s_i)$, where $\delta(\cdot)$ denotes the Dirac delta distribution. Specifically, from (22a) and (22b), we establish

$$\lambda(m) = \frac{1}{N}\sum_{i=0}^{N-1} \ln \sum_{l=1}^{n} p_l Y_l(s_i, m), \tag{24}$$

which reduces to the fixed point analysis presented in Section 3.3 for the case $N = 1$.

If the analytical expression of the probability density function is known, the Lyapunov exponents can be found explicitly. Appendix B specifically illustrates the application of Eq. (22b) to coupled tent maps, which is one of the main results of this paper. Numerical analysis can also benefit from the above formulation, which obviates computational challenges related to uncertainties in rounding variables in Eqs. (6), (7), and (9) for large values of k. This may be especially evident for large curvatures of the individual map, which could result in sudden changes in the synchronization dynamics.

4. The paradigm of the coupled sigmoid maps

Here, we illustrate our approach for the analysis of stochastic synchronization of coupled chaotic maps by focusing on the so-called sigmoid map $S : [0, 1] \to [0, 1]$, see further details in Appendix A. The sigmoid map is a continuously differentiable function, which can be used to proxy logistic and tent maps with parameters 4 and 2, respectively, by varying a single control parameter, see Appendix A.

Lyapunov exponents are computed from Eqs. (6) and (7) for stochastically or statically coupled maps by using a nominal trajectory $s(k)$ generated by initializing a sigmoid map with initial conditions, chosen randomly from the unit interval. In all computations, the argument of the logarithm in (6) and (7) is monitored at each time step to ensure it was above numerical precision. All simulations are performed using MATLAB.

We should comment that the direct computation of the Lyapunov exponent from the time series of the two coupled maps poses further technical challenges [64], related to: (i) the varying size of the invariant manifold as a function of the coupling gain and the switching period; (ii) potential numerical overflow for diverging trajectories; and (iii) false reading for trajectories converging within numerical precision.

The latter possibility should also be contemplated when studying synchronization from the error dynamics rather than the Lyapunov exponent [61] in the case of stochastic switching. For large values of the switching period, it may be possible that the error dynamics reaches values below numerical precision in correspondence of a coupling gain which would support synchronization in case of static coupling. As a result, the two trajectories become identical for all times, irrespective of the sequence of coupling gains. This possibility would lead to incorrectly identifying windows of opportunity.

4.1. Statically coupled maps

As a first step, we investigate the synchronizability of statically coupled maps in terms of the Lyapunov function for their transverse dynamics in (7). Specifically, we evaluate Eq. (7) for different values of the net coupling $d^\star$, ranging from -4 to 4, using a step of 0.001. Simulations are run for 10,000 times steps, the first 10% of the data points are discarded, and the remaining 90% are averaged to estimate the Lyapunov exponent.

Fig. 2 illustrates the dependence of the Lyapunov exponent on the net coupling gain for different values of the control parameter γ, ranging from 1 to 1000. As further elaborated in Appendix B, the selected range of the control parameter γ spans the case of logistic maps ($\gamma = 1$) and approximates the case of tent maps ($\gamma = 1000$). Fig. 2(a) indicates the existence of disjoint intervals of $d^\star$, where the Lyapunov exponent is negative and synchronization is attained, similar to the tent map [63]. The existence, location, and extent of these intervals depend on the parameter γ. For $\gamma = 1$, these intervals do not exist, indicating that logistic maps do not synchronize for any selection of the coupling gains. As γ increases to approximately 10, we observe the formation of two narrow intervals where the maps synchronize.

Such intervals are generally not symmetric with respect to $d^\star = 0$, except for the limit cases of the logistic and tent map, due to the asymmetry in the probability density function, which is elucidated in Appendix A. For the considered cases, we specifically

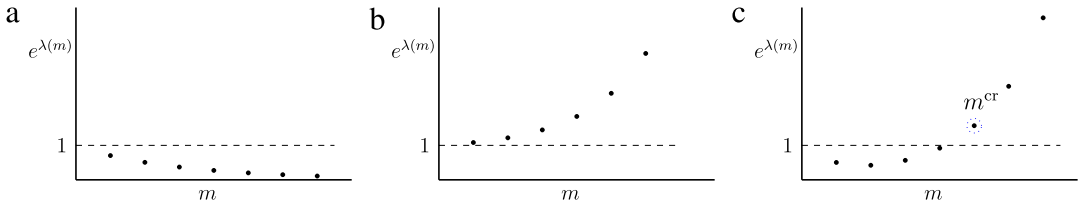

Fig. 1. Stability analysis for fixed points. Lyapunov exponent for the stochastically coupled maps about a fixed point (20), where the net coupling switches between values such that: (a) $\lambda_l^{\mathrm{st}} < 0$ for $l = 1, 2, \ldots, n$; (b) $\bar{\lambda} > 0$; and (c) $\bar{\lambda} < 0$ and $e^{\lambda(1)} < 1$.

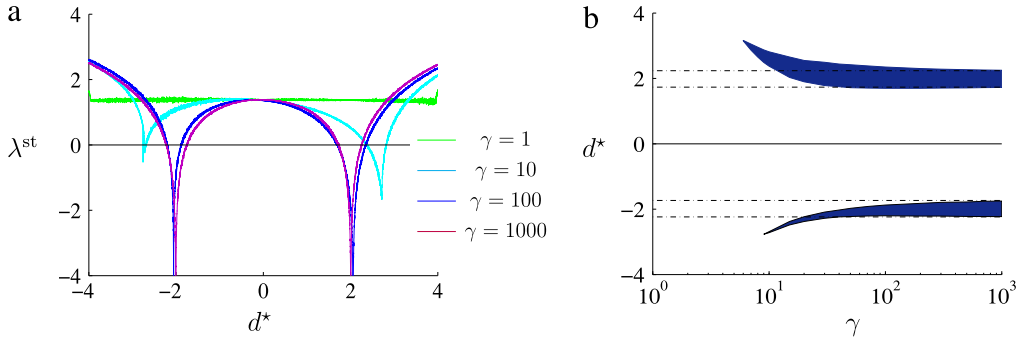

Fig. 2. Synchronizability of statically coupled maps. (a) Lyapunov exponent of the transverse dynamics of two statically coupled sigmoid maps as a function of the net coupling $d^\star$ for different values of the parameter γ. For improved legibility, only values of the Lyapunov exponent larger than -4 are displayed. The dashed line identifies the limit of synchronization $\lambda^{\mathrm{st}} = 0$; and (b) range of the net coupling gain $d^\star$ that is supporting synchronization of the statically coupled sigmoid maps, as a function of the control parameter γ. The dashed line identifies the tent map solution [63].

find that the Lyapunov exponent is negative in the following approximate intervals for $\gamma = 10$, 100, and 1000, respectively: $(-2.72, -2.69)$ and $(2.37, 2.82)$; $(-2.20, -1.87)$ and $(1.70, 2.35)$; and $(-2.23, -1.75)$ and $(1.72, 2.25)$. Fig. 2(a) also shows that the range of the Lyapunov exponent in these intervals is a function of the control parameter γ. Specifically, as γ increases we widen the range of variation of the Lyapunov exponent, which becomes infinitely large as γ goes to infinity and the sigmoid map approaches the tent map. In this case, synchronization may be possible within a single time step.

The role of γ on synchronizability is further illustrated in Fig. 2(b), where we depict the dependence of these intervals on the control parameter γ, which varies with a step of 1 for $\gamma \in [1, 10]$, 10 for $[10, 100]$, and 100 for $[100, 1000]$. Fig. 2 suggests that synchronization becomes feasible for $\gamma = 6$, and that until $\gamma = 9$ only positive values of the net coupling gains ensure synchronization. As γ further increases, we observe that the intervals converge to theoretical predictions from the tent map, that is, $(-\sqrt{5}, -\sqrt{3}) \cup (\sqrt{3}, \sqrt{5})$. In these intervals, the Lyapunov exponent for the tent map is given by [63][2]

$$\lambda^{\mathrm{st}} = \ln|2 - d^\star| + \ln|2 + d^\star|. \tag{25}$$

4.2. Stochastically coupled maps

To elucidate synchronizability of stochastically coupled sigmoid maps, we assume that the net coupling gain d takes values d_1 and d_2 with corresponding probabilities p_1 and $p_2 = 1 - p_1$. This assumption is only intended to ease the illustration of our results, which are applicable to switching on an arbitrary finite sample space D. The numerical computation of the Lyapunov exponent in (6) is performed for different values of d_2 from -4 to 4 with a step of 0.01 and m from 1 to 25 with a step of 1. The probability p_1 is held fixed to 0.5 and the net coupling gain d_1 to -1.90. Further, we consider the same four different values of γ as in Fig. 2.

This wide parameter selection allows for exploring the connection between the stability of synchronization for static coupling and the resulting stochastic synchronization. We consider different cases, where stochastic switching is implemented on coupling gains which could individually support or hamper synchronization for statically coupled maps. Specifically, we contemplate the case in which: none (case I), one (case II), or both (case III) of the coupling gains yield synchronization. Simulations are run for $10^3 \times m$ times steps, the first 10% of the data points are discarded, and the remaining 90% are averaged to estimate the Lyapunov exponent.

Fig. 3 demonstrates the dependence of the Lyapunov exponent on m and d_2 and the selected values of γ, including the logistic map ($\gamma = 1$) and the tent map approximation ($\gamma = 1000$). Therein, the dashed contour identifies the combination of m and d_2 for which the Lyapunov exponent is zero and synchronization initiates. The solid lines depict the values of d_2 for which the effective Lyapunov exponent is zero and synchronization may begin to be feasible based on the necessary condition in Proposition 1. The effective Lyapunov exponent is analytically calculated from the static Lyapunov exponents depicted in Fig. 2 for any value of d_2 and γ. Fig. 4 illustrates the interplay between stochastic synchronization and the stability of synchronization for static coupling, grouped into cases I, II, and III. The possible combinations are identified through different colors, where darker colors (blue and green) mark windows of opportunity and lighter colors (yellow, orange, and red) correspond to asynchronous states.

For $\gamma = 1$, the Lyapunov exponent of the statically coupled logistic maps is positive for any value of the coupling gain (Fig. 2), which corresponds to case I where the switching is implemented between two configurations that would not support synchronization. As a result, there is no value of m which affords synchronization of the coupled logistic maps as shown in Figs. 3(a) and 4(a).

[2] Note that Eq. (25) differs from equation (4.13) in [63] in a factor of 2 which is due to our analysis of mean square error dynamics.

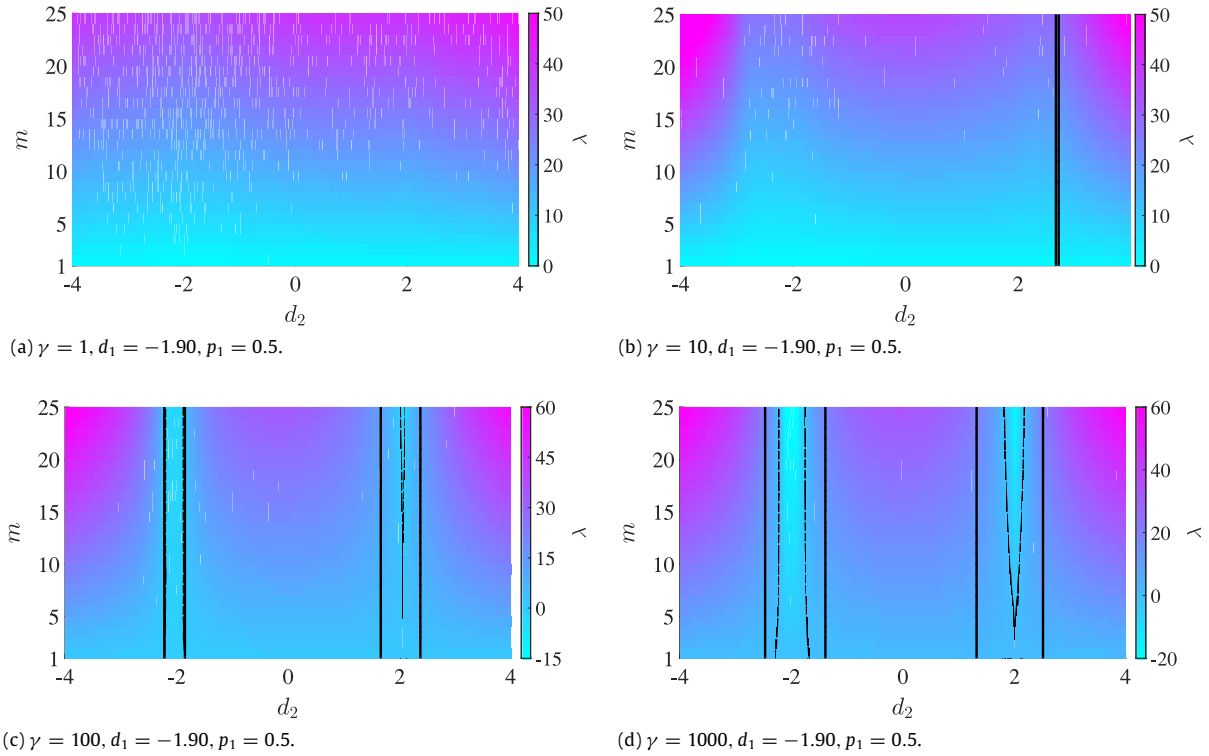

(a) $\gamma = 1, d_1 = -1.90, p_1 = 0.5$.

(b) $\gamma = 10, d_1 = -1.90, p_1 = 0.5$.

(c) $\gamma = 100, d_1 = -1.90, p_1 = 0.5$.

(d) $\gamma = 1000, d_1 = -1.90, p_1 = 0.5$.

Fig. 3. Synchronizability of stochastically coupled maps. Lyapunov exponent of two stochastically coupled sigmoid maps, where the net coupling is switching with equal probability between $d_1 = -1.90$ and d_2 at a period m. Each subfigure refers to a specific value of the control parameter γ, which is varied to elucidate the response of the sigmoid map ($\gamma = 1$) from the logistic to the tent map approximation ($\gamma = 1000$). The color bar illustrates the range of Lyapunov exponents attained for each value of γ. The dashed line identifies the values of d_2 and m for which the Lyapunov exponent is zero; the regions within such contours correspond to negative values of the Lyapunov exponent and thus stochastic synchronization. The solid lines refer to the values of d_2 and m for which the effective Lyapunov exponent is zero, calculated analytically from statically coupled sigmoid maps. The vertical bands identified by such solid lines correspond to regions where stochastic synchronization is feasible, as predicted by Proposition 1. (For interpretation of the references to color in this figure legend, the reader is referred to the web version of this article.)

For $\gamma = 10$, we encompass both cases I and II, depending on the value of d_2, since[3] $\lambda_1^{st} \approx 1.14$ and λ_2^{st} can be negative, as shown in Fig. 2. When applying our necessary condition, we cannot dismiss the possibility of stochastic synchronization, whereby we could attain a negative effective Lyapunov exponent for d_2 between 2.67 and 2.72, as shown in Fig. 3(b). However, the maps do not stochastically synchronize, since the Lyapunov exponent of the stochastically coupled maps is positive for all $m = 1, 2, \ldots, 25$, as displayed in Figs. 3(b) and 4(b).

For $\gamma = 100$ and $\gamma = 1000$, we encompass cases II and III, depending on the value of d_2, since λ_1^{st} is negative ($\lambda_1^{st} \approx -0.10$ for $\gamma = 100$ and $\lambda_1^{st} \approx -0.78$ for $\gamma = 1000$). For both values of γ, we find two intervals of d_2 where the effective Lyapunov exponent, analytically calculated through Proposition 1, is negative. Specifically, it is negative when $(-2.22, -1.85)$ and $(1.66, 2.37)$ for $\gamma = 100$, and $(-2.47, -1.39)$ and $(1.32, 2.51)$ for $\gamma = 1000$, as shown in Fig. 3(c) and (d). Regions of stochastic synchronization are located within these intervals as shown in Fig. 3(c) and (d). For $\gamma = 100$, the effective Lyapunov exponent provides a very close estimate of the region of synchronization in the vicinity for negative values of d_2.

As illustrated in Fig. 4(c) and (d), synchronization may be attained by switching between a coupling gain which supports synchronization and another which does not, as described by case II. This is particularly evident for $\gamma = 1000$, where we observe two thin triangular regions depicted in green where the instability of one of the coupling configurations does not hamper stochastic synchronization. For example, fast switching at $m = 1$ ensures synchronization for d_2 between approximately -2.31 and -1.67, which contains the range where λ_2^{st} is negative, that is, $(-2.23, -1.75)$.

Numerical results in Fig. 4(c) and (d) also indicate that case III, where each coupling configuration would independently lead to synchronization, *does not* guarantee stochastic stability of synchronization for any choice of the switching period. Specifically, for $d_2 > 0$, the region of stochastic synchronization has a wedge-like shape, for which synchronization may only be possible for sufficiently large values of m. Notably, the wedges do not touch the $m = 1$ axis, whereby the stochastic Lyapunov exponents are found to be always positive for m less than 5 and 3 for $\gamma = 100$ and $\gamma = 1000$, respectively. Thus, fast switching between two coupling gains that would individually support synchronization does not produce stochastic synchronization. By increasing the value of m, we confirm our intuition that slowly switching in case III would favor stochastic synchronization, whereby we would trap the trajectory in a static coupling configuration which supports synchronization. By hypothesizing uniform stability of the synchronization manifold for each of the individual values of the net coupling gains, this claim could be proved in the context of the theory of dwell time [68].[4]

Increasing the value of m in the numerical simulations to illustrate the role of slow switching is not feasible, due to the excessive lengths of the time series and resulting challenges in

[3] To reduce the effect of numerical oscillations, values of the Lyapunov exponent in Fig. 2 are estimated by local least square fitting.

[4] While the stability of fixed points could be properly addressed by using dwell time theory, chaotic dynamics pose further challenges associated with the existence of a common Lyapunov function.

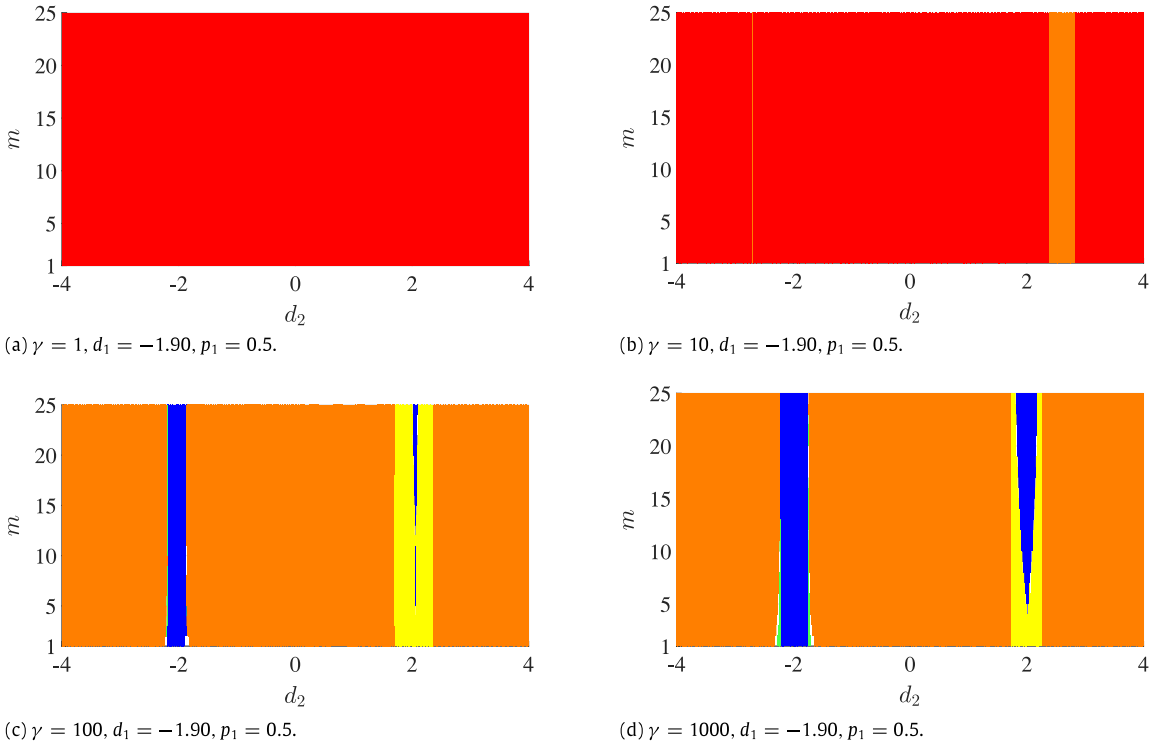

(a) $\gamma = 1, d_1 = -1.90, p_1 = 0.5$.

(b) $\gamma = 10, d_1 = -1.90, p_1 = 0.5$.

(c) $\gamma = 100, d_1 = -1.90, p_1 = 0.5$.

(d) $\gamma = 1000, d_1 = -1.90, p_1 = 0.5$.

Fig. 4. Interplay between synchronization in stochastically and statically coupled maps as in Fig. 3. The stochastic stability of the synchronization manifold for each pair d_2 and m is ascertained from the sign of the Lyapunov exponent in Fig. 3. The partition into cases I, II, and III is based on the sign of the Lyapunov exponent in Fig. 2, corresponding to the net couplings d_1 and d_2. The regions are colored as follows: red (case I); orange (case II without stochastic synchronization); yellow (case III without stochastic synchronization); green (case II with stochastic synchronization); and blue (case III with stochastic synchronization). White coloring identifies pairs of d_2 and m, for which synchronization cannot be precisely assessed due to oscillations in the Lyapunov exponent within ± 0.025. Note that case I prevents the possibility of stochastic synchronization. (For interpretation of the references to color in this figure legend, the reader is referred to the web version of this article.)

estimating the Lyapunov exponents. To address this issue and offer further validation for our claims, we focus on the case $\gamma \to \infty$, which corresponds to the tent map as further elaborated in Appendix A. Not only does the analytical treatment of the tent map address the issue of numerical overflow for long trajectories, but also it enables a closed-form solution of the stochastic Lyapunov exponents. Such an analytical result is critical for accurately resolving the transition between the regions shown in Fig. 4, which can be only approximately predicted through numerical computations.

A closed-form expression for the Lyapunov exponent of coupled tent maps can be derived from Eq. (22b) using the probability density function $\rho(t) = 1$, see Appendix B for a precise derivation,

$$\lambda(m) = \frac{1}{2^m} \sum_{i=0}^{m} \binom{m}{i} \ln \left[\sum_{l=1}^{n} p_l (2 - d_l)^{2(m-i)} (2 + d_l)^{2i} \right]. \tag{26}$$

We comment that for large m the binomial coefficient grows as $2^m/\sqrt{m}$ according to Stirling's formula, which ensures that the summation is well behaved in the slow switching limit [72]. We further note that for zero net coupling gains, the stochastic Lyapunov exponent becomes $2m \ln 2$. This is consistent with Eq. (25), by considering the time re-scaling in Eq. (3).

Fig. 5(a) extends the results presented in Fig. 3(d) by an order of magnitude in m through Eq. (26) specialized to binary switching. The effective Lyapunov exponent is directly computed from Eq. (25), which for the select parameters, $p_1 = p_2 = 0.5$ and $d_1 = -1.9$, is negative in the following intervals for d_2: $\left(-\sqrt{4 + \frac{1}{0.39}}, -\sqrt{4 - \frac{1}{0.39}}\right) \cup \left(\sqrt{4 - \frac{1}{0.39}}, \sqrt{4 + \frac{1}{0.39}}\right)$. Analytical results are in excellent agreement with numerical predictions for $\gamma = 1000$, offering compelling evidence for the accuracy of the proposed closed-form expression and the validity of our computational approach to estimate Lyapunov exponents. Importantly, analytical results for large periods in Fig. 5(b) confirm that slow switching in case III favors stochastic synchronization, whereby we observe that the blue regions vertically extends beyond $m = 25$ as numerically shown in Fig. 4(d). Fig. 5(b) also confirms the existence of a thin green zone surrounding the blue bands, where synchronization is stable even though one of the coupling gains does not support synchronization (case II). For example, in the case of fast switching, $m = 1$, these regions are $(-2.33, -2.24)$ and $(-1.73, -1.64)$ from the closed-form expressions in Eqs. (25) and (26).

The analytical solution in Eq. (26) allows for shedding further light on the possibility of synchronizing coupled maps in case II. Specifically, we consider switching between coupling gains $d_1 = -1.9999$ and $d_2 = 1.7$, which are associated with $\lambda_1^{\text{st}} = -7.82$ (strongly stable synchronization) and $\lambda_2^{\text{st}} = 0.10$ (weakly unstable synchronization). We systematically vary the probability of switching p_1 from 0.6, so that when the coupled maps spend most of the time with the coupling gain that would support synchronization. In this case, the effective Lyapunov exponent is always negative, and synchronization may be attained everywhere in the parameter space.

Surprisingly, under fast switching conditions, synchronization is not attained if $p_1 \lessapprox 1$ as shown in Fig. 6. Although the maps spend most of the time in a configuration that would strongly support synchronization, the sporadic ($p_2 \approx 0$) occurrence of a coupling gain which would lead to weak instability hampers stochastic synchronization under fast switching. Increasing the switching period, synchronization may be attained for $p_1 > 0.995$ (see the "Pinocchio nose" in Fig. 6(b)). For $0.753 < p_1 < 0.795$, we observe a single window of opportunity, whereby synchronization is achieved in a single interval around $m = 10$. For $0.795 < p_1 < 0.824$, a second window of opportunity emerges for smaller values

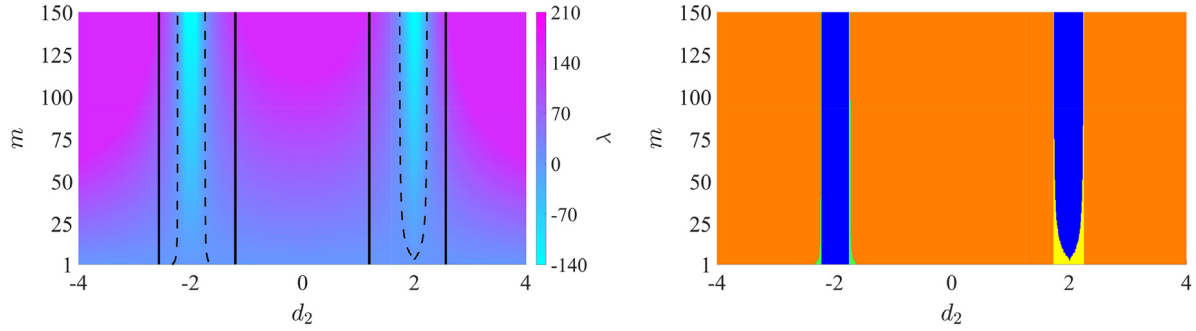

(a) $d_1 = -1.9$, $p_1 = 0.5$. (b) $d_1 = -1.9$, $p_1 = 0.5$.

Fig. 5. Analytical demonstration of slow switching synchronization. (a) Lyapunov exponent of two stochastically tent maps, where the net coupling is switching with equal probability between $d_1 = -1.9$ and d_2 at a period m, analytically computed from Eq. (26). The color bar illustrates the range of Lyapunov exponents attained for each value of γ; for clarity, we have saturated the color bar at 210. The dashed line identifies the values of d_2 and m for which the Lyapunov exponent is zero; the regions within such contours correspond to negative values of the Lyapunov exponent and thus stochastic synchronization. The solid lines refer to the values of d_2 and m for which the effective Lyapunov exponent is zero. The vertical bands identified by such solid lines correspond to regions where stochastic synchronization is feasible, as predicted by Proposition 1. (b) Interplay between synchronization in stochastically and statically coupled tent maps. The partition into cases I, II, and III is based on the sign of the Lyapunov exponent in Eq. (25), corresponding to the net couplings d_1 and d_2. The regions are colored as follows: orange (case II without stochastic synchronization); yellow (case III without stochastic synchronization); green (case II with stochastic synchronization); and blue (case III with stochastic synchronization). (For interpretation of the references to color in this figure legend, the reader is referred to the web version of this article.)

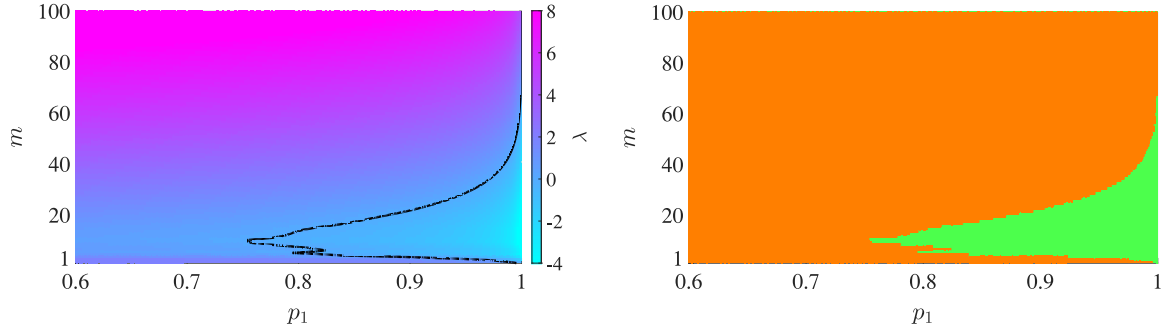

(a) $d_1 = -1.9999$, $d_2 = 1.7$. (b) $d_1 = -1.9999$, $d_2 = 1.7$.

Fig. 6. Analytical demonstration of emergence of windows of opportunity. (a) Lyapunov exponent of two stochastically tent maps as a function of the switching probability p_1 and the period m, analytically computed from Eq. (26) with $d_1 = -1.9999$ and $d_2 = 1.7$. The color bar illustrates the range of Lyapunov exponents attained for each value of γ. The dashed line identifies the values of d_2 and m for which the Lyapunov exponent is zero; the regions within such contours correspond to negative values of the Lyapunov exponent and thus stochastic synchronization. (b) Interplay between synchronization in stochastically and statically coupled tent maps. For the select values of the net couplings, $\lambda_1^{st} = -7.82$ and $\lambda_2^{st} = 0.10$, which correspond to case II. The regions are colored as follows: orange (case II without stochastic synchronization) and green (case II with stochastic synchronization). (For interpretation of the references to color in this figure legend, the reader is referred to the web version of this article.)

of m around 5. The two windows ultimately merge for $p_1 > 0.824$ in a larger window that grows in size as p_1 approaches 1.

While the details of the mechanisms for the appearance of windows of opportunity in stochastically switching networks are yet to be clarified, it is tenable to hypothesize that this effect is related to the dynamic stabilization of an unstable state. From a mechanics perspective, this can be loosely explained by an analogy to the dynamics of Kapitza's pendulum. Kapitza's pendulum is a rigid pendulum in which the pivot point vibrates in a vertical direction, up and down [73]. Stochastic vibrations of the suspension are known to stabilize Kapitza's pendulum in an upright vertical position, which corresponds to an otherwise unstable equilibrium in the absence of suspension vibrations. By this analogy, stochastic switching between stable and unstable configurations can be proposed to perform a similar stabilizing role.

5. Conclusions

While the study of synchronization in evolving dynamical networks has been recently gaining significant momentum, the vast majority of rigorous mathematical investigations focus on the case of fast switching network topology as compared to the individual, intrinsic, node dynamics. In this paper, we have made a first step toward understanding synchronization in stochastically switching networks of coupled maps beyond the fast switching limit.

To isolate the delicate mechanisms underpinning stochastic synchronization, we have considered two coupled maps with independent identically distributed stochastic switching and studied the stability of synchronization as a function of the switching period. We have studied the stochastic stability of the transverse dynamics using the notion of mean square stability, establishing a mathematically-tractable form for the Lyapunov exponent of the error dynamics. We have demonstrated the computation of the stochastic Lyapunov exponent from the knowledge of the probability density function. A necessary condition for stochastic synchronization has been established, aggregating the Lyapunov exponents associated with each static coupling configuration into an effective Lyapunov exponent for the stochastic dynamics. We have focused on the sigmoid map, which bridges the logistic and tent maps as a function of a single control parameter. For tent maps, we have established a closed-form expression for the stochastic Lyapunov exponent, which helps with dissecting the contribution of the coupling gains, switching probabilities, and switching period on stochastic synchronization.

We have demonstrated the central role of non-fast switching, which may provide opportunity for stochastic synchronization in a range of switching periods where fast switching fails to synchronize the maps. More specifically, non-fast switching may

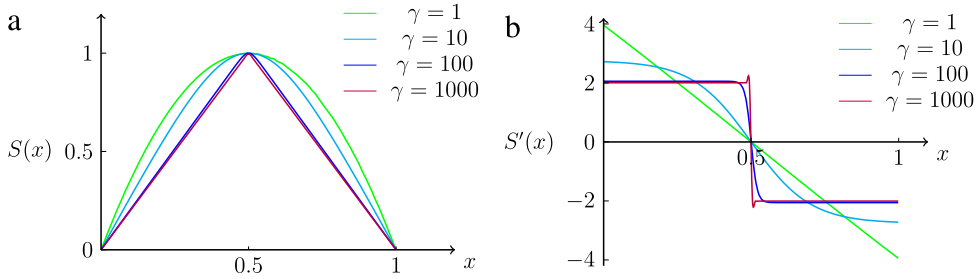

Fig. 7. Sigmoid map (a) and its derivative (b) for different values of γ.

promote synchronization of maps whose coupling alternates between one configuration where synchronization is unstable and another where synchronization is stable (case II). These windows of opportunity for the selection of the switching period may be disconnected and located away from the fast switching limit, where the coupling is allowed to change at each time step.

In contrast to one's expectations, fast switching may not even be successful in synchronizing maps that are coupled by switching between two configurations that would support synchronization (case III). However, a sufficiently slow switching that allows the maps to spend more time in one of the two stable synchronization states will induce stochastic synchronization. The emergence of a lower limit for the switching period to ensure stochastic synchronization is highly non-trivial. On the other hand, the stabilization of synchronization by slow switching in the dwell time limit should be expected, as the maps will spend the time necessary to synchronize in one of the stable configurations, before being re-wired to the other stable configuration.

The proposed necessary condition demonstrates that switching between two unstable states (case I) cannot stabilize synchronization for any switching frequencies, in contrast with networks of continuous-time oscillators where windows of opportunity appear as a result of switching between two unstable (saddle) states. These windows of opportunity for synchronization in continuous-time Rössler and Duffing oscillators [61] and tritrophic Rosenzweig–MacArthur food-chain models [40] were reported earlier, but the derivation of explicit conditions for the emergence of these windows in the continuous-time case is more challenging and remains a subject of future study.

Not only will the continuous-time setting challenge the use of a power expansion in the mean square stability analysis, but also it will increase the dimensionality of the problem. The latter research direction should also be pursued when expanding the framework to large networks, where the relationship between the eigenstructures of the switching Laplacian graphs will likely play a major role. Focusing on a discrete-time setting and scalar maps has enabled us to undertake a first, necessary step toward the prediction and quantification of windows of opportunity for stochastic synchronization beyond fast switching.

Acknowledgments

This work was supported by the US Army Research Office under Grant No. W911NF-15-1-0267 with Drs. Samuel C. Stanton and Alfredo Garcia as the program managers.

Appendix A. Sigmoid map

The sigmoid map is described by the following equation:

$$S(x) = \frac{-\gamma\frac{x}{2} - \ln(1+e^{-\gamma(x-0.5)}) + \ln(1+e^{0.5\gamma})}{-\frac{\gamma}{4} - \ln 2 + \ln(1+e^{\gamma/2})}, \tag{27a}$$

where γ is a parameter that controls the shape of the map. The map is constructed to be an endomorphism in the unit interval. Fig. 7 shows the sigmoid map and its first derivative for a few selected values of the parameter γ.

For values of γ on the order of 1, the first derivative of S is approximately linear, similar to a logistic map with parameter equal to 4, see for example [71]. As γ increases, the curvature of S in the vicinity of $x = 0.5$ increases, and the map approaches the tent map with parameter equal to 2, see for example [71]. Specifically, in the limit $\gamma \to \infty$, the sigmoid map can be approximated by the tent map with parameter equal to 2

$$\begin{cases} 2x, & x \leqslant 0.5 \\ 2(1-x), & x > 0.5 \end{cases} \tag{28}$$

and in the limit $\gamma \to 1$ we recover

$$4x(1-x), \tag{29}$$

the logistic map with parameter equal to 4.

From the time series of the sigmoid map for different values of γ, we can estimate the probability density function $\rho(x)$ associated with the chaotic dynamics. The positive Lyapunov exponents for each of these cases can be obtained from Fig. 2(a) for $d^\star = 0$. From simulation data over 100 000 time steps and binning with a bin size of 0.05, we obtain the probability density functions in Fig. 8. Therein, we also report closed form results for the tent ($\rho(x) = 1$) and the logistic map ($\rho(x) = 1/(\pi\sqrt{x(1-x)})$), see for example [71]. Numerical results confirm analytical predictions for $\gamma = 1$ and indicate close agreement between the sigmoid map and the tent map for $\gamma = 1000$. For intermediate values of γ, we observe a nonsymmetric probability density function with respect to $x = 0.5$.

Appendix B. Lyapunov exponent for stochastically coupled tent maps

Here, we present the derivation of the closed-form expression for the Lyapunov exponent of the stochastically coupled tent maps (26). By using the probability density function $\rho(x) = 1$, Eq. (22b) becomes

$$\lambda(m) = \int_0^1 \ln\left[\sum_{l=1}^{n} p_l Y_l(t,m)\right] dt, \tag{30}$$

where F is given by Eq. (28) and $Y_l(t,m)$ is defined in (23). For convenience, we introduce the 2^m subintervals of $[0,1]$ of length $\frac{1}{2^m}$: $\tau_1 = \left[0, \frac{1}{2^m}\right), \tau_2 = \left(\frac{1}{2^m}, \frac{1}{2^{m-1}}\right), \ldots, \tau_{2^m-1} = \left(\frac{2^m-1}{2^{m-1}}, \frac{2^m-1}{2^m}\right), \tau_{2^m} = \left(\frac{2^m-1}{2^m}, 1\right]$. These subintervals constitute a partition of the unit interval up to a set of measure zero, where $Y^l(t,m)$ is not uniquely defined as detailed below.

For each of these subintervals, we can determine the sequence of composite functions that is needed for calculating $Y_l(t,m)$ in the following way. For $t \in \tau_1$ we find $F^0(t) = t < \frac{1}{2^m}$. This quantity is

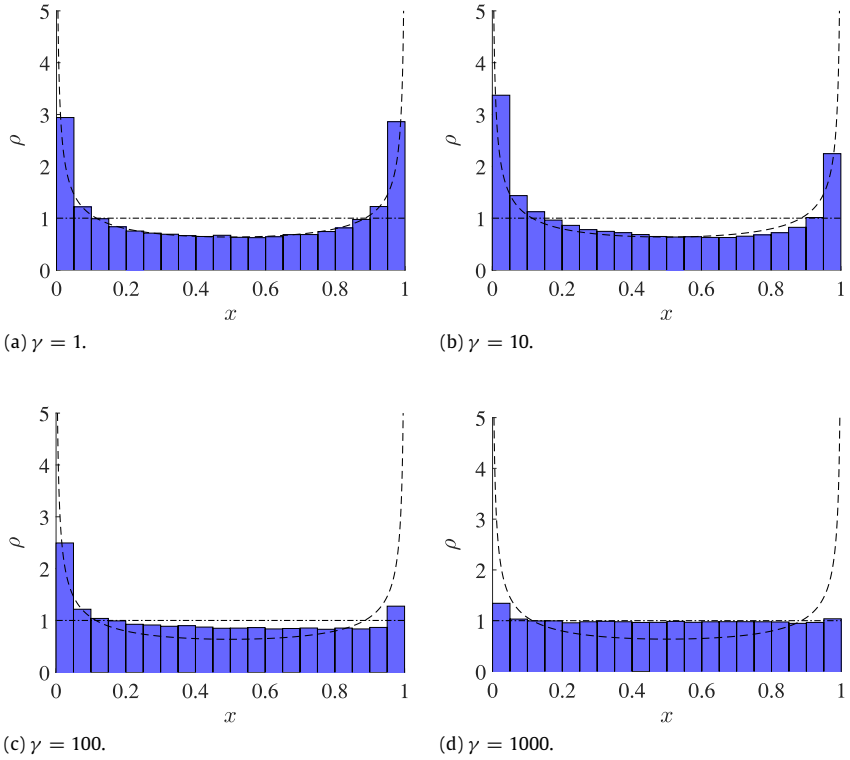

(a) $\gamma = 1$. (b) $\gamma = 10$.

(c) $\gamma = 100$. (d) $\gamma = 1000$.

Fig. 8. Asymmetric ergodic behavior of the sigmoid map. Probability density functions of the sigmoid map (27a) for different values of the control parameter γ: (a) $\gamma = 1$, (b) $\gamma = 10$, (c) $\gamma = 100$, and (d) $\gamma = 1000$. Probability density function of the tent and logistic maps are shown as dot-dashed and dashed lines, respectively.

less than 0.5, thereby from (26), we find $F^1(t) = 2F^0(t)$, which is, in turn, less than $2\frac{1}{2^m}$. The latter quantity is again less than 0.5 and the argument above can be iterated for any composite function up to the $(m-1)$th order. As a result, within τ_1, $F'(F^i(t))$ will be equal to 2 for $i = 0, 1, \ldots, m-1$, and $Y_l(t, m)$ reduces to $(2 - d_l)^{2m}$.

Following a similar line of argument, we can study the sequence of composite functions for $t \in \tau_2$. In this case, we find $F^i(t) < 0.5$ for $i = 0, 1, \ldots, m-2$ and $F^{m-1}(t) > 0.5$. Thus, $F'(F^i(t))$ will be equal to 2 for $i = 0, 1, \ldots, m-2$ and -2 for $i = m-1$, which imply that $Y_l(t, m) = (2 - d_l)^{2(m-1)}(2 + d_l)^2$. Note that this value is different from the value attained in τ_1, confirming that $Y_l(t, m)$ jumps between two contiguous subintervals.

By carrying out this procedure for all of the considered 2^m subintervals, we find that $Y_l(t, m)$ is constant in each subinterval and equal to one of the following values: $Y_l^{(0,m)} = (2 - d_l)^{2m}$, $Y_l^{(1,m)} = (2 - d_l)^{2(m-1)}(2 + d_l)^2, \ldots, Y_l^{(i,m)} = (2 - d_l)^{2(m-i)}(2 + d_l)^{2i}, \ldots, Y_l^{(m,m)} = (2 + d_l)^{2m}$. Each of these values occurs $\binom{m}{i}$ times, corresponding to the number of possible ways to obtain $(2 - d_l)^{2i}(2 + d_l)^{2(m-i)}$ from the product of m quantities each taking values in $\{(2 - d_l)^2, (2 + d_l)^2\}$.

By partitioning the integral in Eq. (30) in 2^m integrals over $\tau_1, \ldots, \tau_{2^m}$, we obtain

$$\lambda(m) = \sum_{i=1}^{2^m} \int_{\tau_i} \ln \left[\sum_{l=1}^{n} p_l Y_l(t, m) \right] dt = \frac{1}{2^m} \sum_{i=0}^{m} \binom{m}{i} \ln \left[\sum_{l=1}^{n} p_l Y_l^{(i,m)} \right], \tag{31}$$

which implies Eq. (26).

References

[1] R. Albert, A.L. Barabási, Statistical mechanics of complex networks, Rev. Mod. Phys. 74 (1) (2002) 49–98.

[2] S. Boccaletti, V. Latora, Y. Moreno, M. Chaovez, D.-U. Hwanga, Complex networks: structure and dynamics, Phys. Rep. 424 (4–5) (2006) 175–308.

[3] S. Dorogovtsev, J.F.F. Mendes, Evolution of networks, Adv. Phys. 51 (4) (2002) 1079–1187.

[4] M. Newman, The structure and function of complex networks, SIAM Rev. 45 (2) (2003) 167–256.

[5] S.H. Strogatz, Exploring complex networks, Nature 410 (6825) (2001) 268–276.

[6] M. Barahona, L. Pecora, Synchronization in small-world systems, Phys. Rev. Lett. 89 (5) (2002) 054101.

[7] I. Belykh, M. di Bernardo, J. Kurths, M. Porfiri, Evolving dynamical networks, Physica D 267 (1) (2014) 1–6.

[8] V.N. Belykh, I.V. Belykh, M. Hasler, Connection graph stability method for synchronized coupled chaotic systems, Physica D 195 (1) (2004) 159–187.

[9] S. Boccaletti, J. Kurths, G. Osipov, D. Valladares, C. Zhou, The synchronization of chaotic systems, Phys. Rep. 366 (1) (2002) 1–101.

[10] P. DeLellis, M. di Bernardo, T.E. Gorochowski, G. Russo, Synchronization and control of complex networks via contraction, adaptation and evolution, IEEE Circuits Syst. Mag. 10 (3) (2010) 64–82.

[11] L.M. Pecora, T.L. Carroll, Master stability functions for synchronized coupled systems, Phys. Rev. Lett. 80 (10) (1998) 2109.

[12] T. Nishikawa, A. Motter, Network synchronization landscape reveals compensatory structures, quantization, and the positive effect of negative interactions, Proc. Natl. Acad. Sci. USA 107 (2010) 10342.

[13] A. Pikovsky, M. Rosenblum, J. Kurths, Synchronization: a Universal Concept in Nonlinear Sciences, Vol. 12, Cambridge University Press, Cambridge, UK, 2003.

[14] R. Amritkar, C. Hu, Synchronized state of coupled dynamics on time-varying networks, Chaos 16 (1) (2006) 015117.

[15] A. Azzouz, M. Hasler, Uniqueness of the asymptotic behavior of autonomous and non-autonomous, switched and non-switched, linear and nonlinear systems of dimension 2, Int. J. Circuit Theory Appl. 16 (2) (1988) 191–226.

[16] Y. Bakhtin, T. Hurth, J.C. Mattingly, Regularity of invariant densities for 1D systems with random switching, Nonlinearity 28 (11) (2015) 3755–3787.

[17] L. Chen, C. Qin, H. Huang, Synchronization with on-off coupling: role of time scales in network dynamics, Phys. Rev. E 79 (4) (2009) 045101.

[18] P. De Lellis, M. di Bernardo, F. Garofalo, Synchronization of complex networks through local adaptive coupling, Chaos 18 (3) (2008) 037110.

[19] L. Fortuna, M. Frasca, A. Rizzo, Experimental pulse synchronisation of two chaotic circuits, Chaos Solitons Fractals 17 (2) (2003) 355–361.

[20] T. Gorochowski, M. di Bernardo, C. Grierson, Evolving enhanced topologies for the synchronization of dynamical complex networks, Phys. Rev. E 81 (5) (2010) 056212.

[21] J. Ito, K. Kaneko, Spontaneous structure formation in a network of chaotic units with variable connection strengths, Phys. Rev. Lett. 88 (2002) 028701.

[22] L. Kocarev, P. Janjić, U. Parlitz, T. Stojanovski, Controlling spatio-temporal chaos in coupled oscillators by sporadic driving, Chaos Solitons Fractals 9 (1) (1998) 283–293.
[23] S.D. Lawley, J.C. Mattingly, M.C. Reed, Sensitivity to switching rates in stochastically switched ODEs, Commun. Math. Sci. 12 (7) (2014) 1343–1352.
[24] R. Leander, S. Lenhart, V. Protopopescu, Controlling synchrony in a network of Kuramoto oscillators, Physica D 301–302 (2015) 36–47.
[25] J. Lü, G. Chen, A time-varying complex dynamical network model and its controlled synchronization criteria, IEEE Trans. Automat. Control 50 (6) (2005) 841–846.
[26] J. Lu, D. Hill, Impulsive synchronization of chaotic Lur'e systems by linear static measurement feedback: an LMI approach, IEEE Trans. Circuits Syst. II 54 (8) (2007) 710–714.
[27] J.D. Skufca, E.M. Bollt, Communication and synchronization in disconnected networks with dynamic topology: moving neighborhood networks, Math. Biosci. Eng. 1 (2) (2004) 347.
[28] P. So, B. Cotton, E. Barreto, Synchronization in interacting populations of heterogeneous oscillators with time-varying couplings, Chaos (3) (2008) 037114. 18.
[29] F. Sorrentino, E. Ott, Adaptive synchronization of dynamics on evolving complex networks, Phys. Rev. Lett. 100 (11) (2008) 114101.
[30] D.J. Stilwell, E.M. Bollt, D.G. Roberson, Sufficient conditions for fast switching synchronization in time-varying network topologies, SIAM J. Appl. Dyn. Syst. 5 (1) (2006) 140–156.
[31] T. Stojanovski, L. Kocarev, U. Parlitz, R. Harris, Sporadic driving of dynamical systems, Phys. Rev. E 55 (4) (1997) 4035–4048.
[32] D.H. Zanette, A.S. Mikhailov, Dynamical systems with time-dependent coupling: clustering and critical behavior, Physica D 194 (3) (2004) 203–218.
[33] I.V. Belykh, V.N. Belykh, M. Hasler, Blinking model and synchronization in small-world networks with a time-varying coupling, Physica D 195 (1) (2004) 188–206.
[34] M. Hasler, I. Belykh, Blinking long-range connections increase the functionality of locally connected networks, IEICE Trans. Fundam. Electron. Commun. Comput. Sci. 88 (10) (2005) 2647–2655.
[35] A. Mondal, S. Sinha, J. Kurths, Rapidly switched random links enhance spatiotemporal regularity, Phys. Rev. E 78 (6) (2008) 066209.
[36] M. Porfiri, D.J. Stilwell, E.M. Bollt, Synchronization in random weighted directed networks, IEEE Trans. Circuits Syst. I 55 (10) (2008) 3170–3177.
[37] M. Porfiri, D.J. Stilwell, E.M. Bollt, J.D. Skufca, Random talk: random walk and synchronizability in a moving neighborhood network, Physica D 224 (1) (2006) 102–113.
[38] D. Mills, Internet time synchronization: the network time protocol, IEEE Trans. Commun. 10 (10) (1991) 1482–1493.
[39] C. Tse, M. Di Bernardo, Complex behavior in switching power converters, Proc. IEEE 90 (2002) 768–781.
[40] R. Jeter, I. Belykh, Synchrony in metapopulations with sporadic dispersal, Int. J. Bifurcation Chaos 25 (7) (2015) 1540002.
[41] M. Frasca, A. Buscarino, A. Rizzo, L. Fortuna, S. Boccaletti, Synchronization of moving chaotic agents, Phys. Rev. Lett. 100 (4) (2008) 044102.
[42] D.J.T. Sumpter, Collective Animal Behavior, Princeton University Press, Princeton, NJ, USA, 2010.
[43] M. Porfiri, F. Fiorilli, Global pulse synchronization of chaotic oscillators through fast-switching: theory and experiments, Chaos Solitons Fractals 41 (1) (2009) 245–262.
[44] M. Porfiri, F. Fiorilli, Node-to-node pinning-control of complex networks, Chaos 19 (1) (2009) 013122.
[45] M. Porfiri, F. Fiorilli, Experiments on node-to-node pinning control of Chua's circuits, Physica D 239 (8) (2010) 454–464.
[46] M. Porfiri, R. Pigliacampo, Master–slave global stochastic synchronization of chaotic oscillators, SIAM J. Appl. Dyn. Syst. 7 (3) (2008) 825–842.
[47] M. Porfiri, D.J. Stilwell, Consensus seeking over random weighted directed graphs, IEEE Trans. Automat. Control 52 (9) (2007) 1767–1773.
[48] N. Abaid, I. Igel, M. Porfiri, On the consensus protocol of conspecific agents, Linear Algebra Appl. 437 (1) (2012) 221–235.
[49] N. Abaid, M. Porfiri, Consensus over numerosity-constrained random networks, IEEE Trans. Automat. Control 56 (3) (2011) 649–654.
[50] N. Abaid, M. Porfiri, Leader-follower consensus over numerosity-constrained random network, Automatica 48 (8) (2012) 1845–1851.
[51] S.H. Lee, V. Kapila, M. Porfiri, A. Panda, Master–slave synchronization of continuously and intermittently coupled sampled-data chaotic oscillators, Commun. Nonlinear Sci. Numer. Simul. 15 (12) (2010) 4100–4113.
[52] V. Mwaffo, R.P. Anderson, M. Porfiri, Collective dynamics in the Vicsek and vectorial network models beyond uniform additive noise, J. Nonlinear Sci. 25 (5) (2015) 1053–1076.
[53] V. Mwaffo, P. DeLellis, M. Porfiri, Criteria for stochastic pinning control of networks of chaotic maps, Chaos 24 (1) (2014) 013101.
[54] V. Mwaffo, M. Porfiri, Linear analysis of the vectorial network model in the presence of leaders, Automatica 58 (2015) 160–166.
[55] M. Porfiri, A master stability function for stochastically coupled chaotic maps, Europhys. Lett. 96 (4) (2011) 40014.
[56] M. Porfiri, Stochastic synchronization in blinking networks of chaotic maps, Phys. Rev. E 85 (5) (2012) 056114.
[57] M. Porfiri, Linear analysis of the vectorial network model, IEEE Trans. Circuits Syst. II 61 (1) (2014) 44–48.
[58] I. Belykh, V. Belykh, R. Jeter, M. Hasler, Multistable randomly switching oscillators: the odds of meeting a ghost, Eur. Phys. J. Spec. Top. 222 (10) (2013) 2497–2507.
[59] M. Hasler, V. Belykh, I. Belykh, Dynamics of stochastically blinking systems. Part I: finite time properties, SIAM J. Appl. Dyn. Syst. 12 (2) (2013) 1007–1030.
[60] M. Hasler, V. Belykh, I. Belykh, Dynamics of stochastically blinking systems. Part II: asymptotic properties, SIAM J. Appl. Dyn. Syst. 12 (2) (2013) 1031–1084.
[61] R. Jeter, I. Belykh, Synchronization in on-off stochastic networks: windows of opportunity, IEEE Trans. Circuits Syst. I 62 (5) (2015) 1260–1269.
[62] R. Jeter, I. Belykh, Dynamical networks with on-off stochastic connections: beyond fast switching, in: IEEE International Symposium on Circuits and Systems, (ISCAS), IEEE, 2014, pp. 1788–1791.
[63] M. Hasler, Y.L. Maistrenko, An introduction to the synchronization of chaotic systems: coupled skew tent maps, IEEE Trans. Circuits Syst. I 44 (10) (1997) 856–866.
[64] A. Pikovsky, A. Politi, Lyapunov Exponents: a Tool to Explore Complex Dynamics, Cambridge University Press, Cambridge, UK, 2016.
[65] Y. Fang, Stability analysis of linear control (Ph.D. thesis), Case Western Reserve University, Cleveland, OH, USA, 1994.
[66] H.J. Kushner, Introduction to Stochastic Control, Holt, Rinehart and Winston, New York, 1971.
[67] P.S. Bullen, D.S. Mitrinovic, M. Vasic, Means and their Inequalities, Vol. 31, Springer-Science+Business Media, B. V., Dordrecht, Holland, 1987.
[68] Z. Sun, Switched Linear Systems: Control and Design, Springer-Verlag, London, UK, 2006.
[69] L. Bunimovich, S. Dani, R. Dobrushin, M. Jakobson, I. Kornfeld, N. Maslova, Y. Pesin, Y. Sinai, J. Smillie, Y. Sukhov, A. Vershik, Dynamical Systems, Ergodic Theory and Applications, second ed., in: Encyclopaedia of Mathematical Sciences, Springer-Verlag, Berlin, Germany, 2000.
[70] L. Billings, E.M. Bollt, Probability density functions of some skew tent maps, Chaos Solitons Fractals 12 (2) (2001) 365–376.
[71] E.M. Bollt, N. Santitissadeekorn, Applied and Computational Measurable Dynamics, Vol. 18, SIAM, Philadelphia, PA, USA, 2013.
[72] F.W.J. Oliver, D.W. Lozier, R.F. Boisvert, C.W. Clark (Eds.), NIST Handbook of Mathematical Functions, Cambridge University Press, New York, NY, USA, 2010.
[73] P.L. Kapitza, Dynamic stability of a pendulum when its point of suspension vibrates, Sov. Phys. JETP 21 (1951) 588–592.